

Robust Sampled–Data Control of Hydraulic Flight Control Actuators

Dipl.–Ing. Markus Gustav Kliffken
Section Aircraft–Systems Engineering
Technical Univerisity Hamburg–Harburg
Neßpiel 5, D-21129 Hamburg, Germany

Tel.: ++49(+40)74315–212 Fax: –270
Email: Kliffken@tu-harburg.d400.de
<http://www.tu-harburg.de/fst/FST.Kliffken.html>

Abstract

In todays Fly–by–Wire systems the primary flight control surfaces of modern commercial and transport aircraft are driven by electro hydraulic linear actuators. Changing flight conditions as well as nonlinear actuator dynamics may be interpreted as parameter uncertainties of the linear actuator model. This demands a robust design for the controller.

Here the *Parameter Space Design* is used for the direct sampled–data controller synthesis. Therefore, a static output controller is choosen, the model discretized by approximation and the specifications represented by eigenvalue location. Simultaneous Γ –stabilisation allows a graphical controller selection.

With realistic assumptions, the positioning system of control surfaces corresponds to conventional hydraulic actuation. The relevant uncertain parameters of the time–continuous linear model are the hydraulic damping and eigenfrequency. Avoiding a feedback for the servo valve and predesigning the position feedback gain due to the specified bandwidth, the velocity and acceleration feedback gain follow from direct pole region assignment. It follows that here only the velocity feedback gain is required. For the generation of the velocity signal a digital differential filter is applied. Simulation results in time– and frequency–domain shows the improvement by the choosen robust controller.

Keywords: Primary Flight Control System, Hydraulic Linear Actuators, Sampled-Data Control, Robust Control, Parameter Space Design.

1 Introduction

Due to the high power density the primary flight control surfaces (see fig. 1) of modern commercial and transport aircraft are driven by hydraulic linear servo actuators. In Fly-by-Wire systems they are controlled fully electrical and digital by the flight control computer, which distinguishes to newest tendencies [4]. Today, as a result of the low performance requirements classic porportional controllers often suffice. Future projects — like very large aircraft with flexible structures — will need improved positioning behavior.

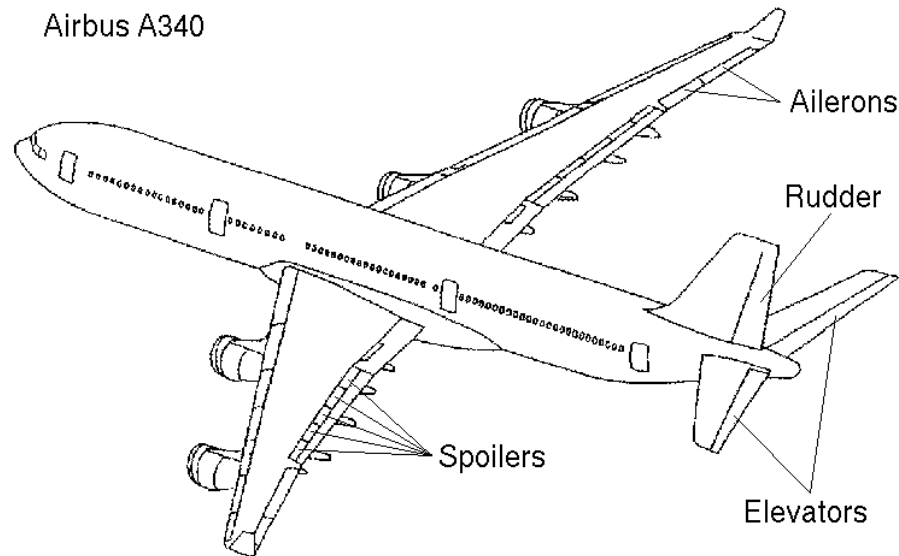


Figure 1: Primary Flight Control of the *Airbus A340*

The physical parameters of the actuator vary because of changing flight conditions, like temperature, flight altitude or true air speed, and the natural aging during the long operation time. Additional system nonlinearities can be interpreted as parameter uncertainties as well, if they are not too dynamical. This demands a robust design for a linear controller.

As a typical example of an electro hydraulic actuation system, the inboard aileron of the *Airbus A330/340* is used. Its functions and parameters are published in [6] and well known from actuator and aircraft manufacturers. The progress reports [12, 13] describe the presented and additional aspects more detailed.

2 Parameter Space Design

For an enhanced and robust controller synthesis the *Parameter Space Design* is used. This method is mostly established by *J. Ackermann* and deccribed in detail in his books [2, 3]. Here, only those facts are briefly discussed, which are necessary and applied for the synthesis of the actuator control. Further details on sampled-data control explain [2, 9].

2.1 Uncertain Plant Description

The time–continuous model for the single–input *plant family* is given as a linear time–invariant system in general state–space description

$$\begin{aligned}\dot{\mathbf{x}}_{(n)}(t) &= \mathbf{A}_{(n,n)}(\mathbf{q}) \cdot \mathbf{x}_{(n)}(t) + \mathbf{b}_{(n)}(\mathbf{q}) \cdot u(t) \\ \mathbf{y}_{(q)}(t) &= \mathbf{C}_{(n,q)}(\mathbf{q}) \cdot \mathbf{x}_{(n)}(t) .\end{aligned}\quad (1)$$

Herein \mathbf{A} represents the system matrix, \mathbf{b} the input vector, \mathbf{C} the output matrix, \mathbf{x} the state vector, \mathbf{y} the output vector and u the input. Their indices indicate the dimensions, as well as the argument t denotes the time–dependency and \mathbf{q} the parameter–dependency, respectively.

The vector $\mathbf{q} = [q_1 \cdots q_l]^T$ collects all l time–independent and real *uncertain parameters* which vary between their lower and upper bound $q_i \in [q_i^-; q_i^+]$. Really independent uncertain parameters in the *operation domain* form an hyperrectangle in the *uncertainty domain*: the *parameter box*

$$Q = \{ \mathbf{q} \mid q_i \in [q_i^-; q_i^+], i = 1, 2, \dots, l \} . \quad (2)$$

Thereby physically motivated parameter uncertainties prevent for conservative over–boundings. Mostly only a finit number of operation points $\mathbf{q}^{(j)} \in Q$ are of interest, i.e. the corners of Q . Thus the hole plant family (1) yields $j = 1, \dots, J$ different models

$$\begin{aligned}\dot{\mathbf{x}}(t) &= \mathbf{A}^{(j)} \cdot \mathbf{x}(t) + \mathbf{b}^{(j)} \cdot u(t) \\ \mathbf{y}(t) &= \mathbf{C}^{(j)} \cdot \mathbf{x}(t) .\end{aligned}\quad (3)$$

2.2 Time–Discretization

Assuming the usual sampler with zero order hold, the time–continuous system (1) yields the time–discretized system

$$\begin{aligned}\mathbf{x}(kT + T) &= \mathbf{A}_d(\mathbf{q}) \cdot \mathbf{x}(kT) + \mathbf{b}_d(\mathbf{q}) \cdot u(kT) \\ \mathbf{y}(kT) &= \mathbf{C}(\mathbf{q}) \cdot \mathbf{x}(kT) ,\end{aligned}\quad (4)$$

by using the solution of the state–space differential equation at the sampling instance $t = kT$. Herein the time–discret system matrix \mathbf{A}_d represents the homogeneous solution and the time–discret input vector \mathbf{b}_d the inhomogeneous solution. The output matrix $\mathbf{C}(\mathbf{q})$ is identical for both systems (1) and (4).

Due to the mostly lost clearness by algebraic time–discretization, approximation techniques have been established. Based on *Tustin's method*, a state–space description can be approximated by

$$\mathbf{A}_d \approx \left[\mathbf{I} + \frac{\mathbf{A}T}{2} \right] \cdot \left[\mathbf{I} - \frac{\mathbf{A}T}{2} \right]^{-1} \quad \text{and} \quad \mathbf{b}_d \approx \left[\mathbf{I} - \frac{\mathbf{A}T}{2} \right]^{-1} \cdot \mathbf{b}T , \quad (5)$$

which is only practical for fast sampling.

Choosing the sample time T , it is to consider that the system controllability is not lost for every possible operation point $\mathbf{q}^{(j)}$ in the uncertainty domain Q . Therefore the sampling theorem must always be fulfilled.

2.3 Control law

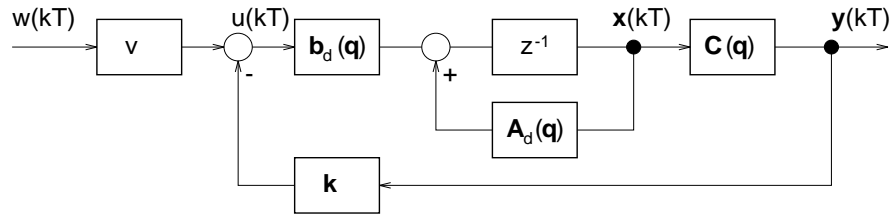


Figure 2: Sampled-data control loop

Here a static output control law

$$u(kT) = -\mathbf{k}^T \cdot \mathbf{y}(kT) + v \cdot w(kT) , \quad (6)$$

with the control vector $\mathbf{k} = [k_1 \cdots k_q]^T$, the prefilter v and the demand $w(kT)$, is assumed, see fig. 2. Applying the controller (6) to the plant (4) the closed-loop system possess the uncertain characteristic polynomial

$$p_d(z, \mathbf{q}, \mathbf{k}) = \det(z \cdot \mathbf{I} - \mathbf{A}_d(\mathbf{q}) - \mathbf{b}_d(\mathbf{q}) \cdot \mathbf{k}^T \cdot \mathbf{C}(\mathbf{q})) = [1 z \cdots z^n] \cdot \mathbf{a}_d(\mathbf{q}) , \quad (7)$$

with the vector of the polynomial coefficients $\mathbf{a}_d = [a_0 a_1 \cdots a_n]^T$.

While measuring the regulated variable is unavoidable, additional sensors are mostly not desired. Traditional state estimation by an observer or a Kalman filter is sometimes unsuitable, because they depend on the model of an uncertain plant. However, low pass filtered differentiation allows easily the robust generation of derivations of measured states. A digital filter for differentiation can be designed through impuls invariant synthesis [16]. Its odd order transfer function with $d = 1, 3, \dots$ yields by series expansion

$$G_D(z) = \frac{4 z^{-[\frac{d+1}{2}]}}{\pi T} \cdot \sum_{k=1}^{[\frac{d+1}{2}]} \frac{-1^{k+1}}{[2k-1]^2} \cdot [z^k - z^{1-k}] . \quad (8)$$

2.4 Specification

Typical control loop specifications are often given in time domain for the step response or in frequency domain for the bode plot. Both can be represented by eigenvalue locations too. Applying a constant controller to an uncertain plant the pole placement degenerates to *pole region assignment*. These regions name Γ and their boundary $\partial\Gamma$.

For time-continuous systems a common region Γ is a hyperbola in the s -plane, which guarantees minimal damping and bandwidth. Similar simple regions in the z -plane $z = \sigma + j\omega$ are circles

$$(\sigma - \sigma_0)^2 + \omega^2 = r^2 \quad (9)$$

with $\sigma \in [\sigma_0 - r^2; \sigma_0 + r]$ and the central point

$$\sigma_0 = \begin{cases} r & : 0 \leq r \leq 0.5 \\ 1 - r & : 0.5 \leq r \leq 1 \\ 0 & : 1 \leq r \end{cases}$$

for different radii r . Table 1 shows the approximate correspondence between the minimal damping D^- as well as radii r and central point σ_0 of a circle for Γ .

D^-	0	0.35	0.5	0.7
r	1	0.5	0.44	0.33
σ_0	0	0.5	0.44	0.33

Table 1: Damping, radii and central point

2.5 Simultaneous Γ -Stabilisation

Now, the goal is designing a controller so that the closed-loop system, represented by the characteristic polynomial, has the specified stability performance for the total uncertainty domain.

Therefore the complete uncertain plant family (4) is to transform into the controller plane. This presents for each operation point $\mathbf{q}^{(j)}$ a set of possible controllers, which places the eigenvalues of the characteristic polynomial $p_d(z, \mathbf{k}, \mathbf{q})$ into Γ .

$$K_\Gamma^{(j)} = \left\{ \mathbf{k} \mid p_d(z, \mathbf{q}^{(j)}, \mathbf{k}) = \prod_{i=1}^n [z - z_i^{(j)}] \wedge z_i^{(j)} \in \Gamma, \text{ with } j = 1, \dots, J \right\} \quad (10)$$

The intersection of all controller sets

$$K_\Gamma = \bigcap_{j=1}^J K_\Gamma^{(j)} \quad (11)$$

represents the set of the simultaneous Γ -stabilizing controllers. Figure 3 illustrates the method for $J = 2$ operation points and $q = 2$ controller gains.

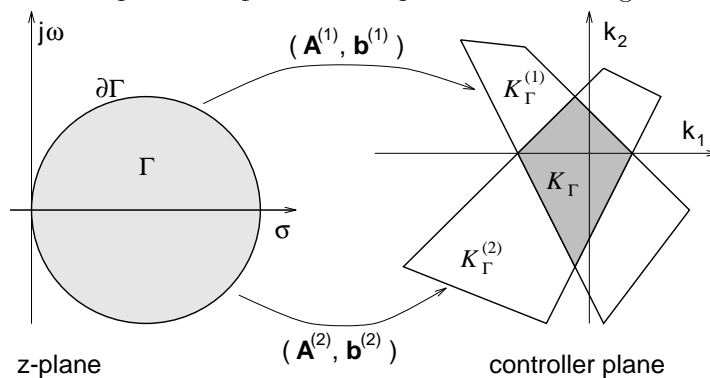


Figure 3: Simultaneous Γ -stabilisation

For an empty intersection $K_\Gamma = \{ \}$ the specifications Γ can not be fulfilled. Additional freedoms in the controller selection $\mathbf{k} \in K_\Gamma$ allow additional design requirements, e.g.: small controller norm $\|\mathbf{k}\|$ in order to small input signals $|u(kT)|$, safety margin for controller \mathbf{k} away from the boundaries of K_Γ , robustness with respect to sensor failures [14] and gain reduction margins. Finally the chosen controller \mathbf{k} should be analysed and proven, e.g. by nonlinear simulation or/and realistic tests — especially if system nonlinearities are interpreted as parameter uncertainties or/and dynamics neglected.

2.6 Pole Region Assignment

In case of only two free controller gains $\mathbf{k} = [k_1 \ k_2]^T$ a direct pole region assignment is possible. Therefore the *Boundary Representation Theorem* is very useful, because it offers a direct solution, which can be solved analytically with computer algebra [7, 13, 14].

The *complex root boundary* represents those combinations of both gains, which produce conjugate complex poles on $\partial\Gamma$. Their parametric representation in the controller plane $(k_1(\alpha), k_2(\alpha))$ yields

$$\begin{bmatrix} d_0(\alpha) & d_1(\alpha) & \cdots & d_n(\alpha) \\ 0 & d_0(\alpha) & \cdots & d_{n-1}(\alpha) \end{bmatrix} \cdot \mathbf{a}^{(j)} \equiv \begin{bmatrix} 0 \\ 0 \end{bmatrix}. \quad (12)$$

Herein α parameterizes the boundary $\partial\Gamma : z = \sigma(\alpha) + j\omega(\alpha)$ and the elements are its function

$$\begin{aligned} d_0(\alpha) &= 1 \\ d_1(\alpha) &= 2\sigma(\alpha) \\ d_{i+1}(\alpha) &= 2\sigma(\alpha)d_i(\alpha) - [\sigma(\alpha)^2 + \omega(\alpha)^2]d_{i-1}(\alpha) \end{aligned}$$

with $i = 1, \dots, n - 1$. Every intersection of the boundary $\partial\Gamma$ and the real axis σ_j of the z -plane forms a *real root boundary*. Its parametrization follows by evaluating the characteristic polynomial at the intersection

$$p_d(z = -\sigma_j, \mathbf{q}, \mathbf{k}) \equiv 0. \quad (13)$$

3 Surface/Aktuator Control

While [17] presents a survey on flight control actuation, [6] describes especially the primary flight control of the *Airbus A330/340* and [11] traditional controller design of hydraulic linear actuators. The results of the authors research project summarize the progress reports [12, 13] and additional papers [14, 15]

3.1 Positioning Actuation System

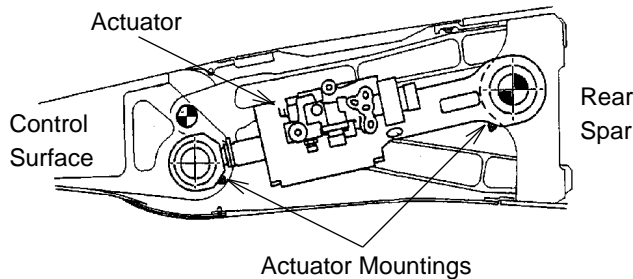


Figure 4: Actuator installation

Figure 4 shows the installation of one of two actuators for the inboard aileron. Here one actuator is active and rotates the surface by translating, while the other actuator is by-passed and operates as a damper. With the first fault they change

their operation conditions and with the second both act as dampers, to prevent flutter [8].

Figure 5 shows a simplified model sketch of an active actuator. Here the inertial of the surface is reduced to the effective mass m_{\perp} , where the damping actuator f_D , the aerodynamic load by a systematic hinge moment f_L and disturbance loads f are applied. The actuator with the two volumes $V_{A,B}$ and pressures $p_{A,B}$ displaces the reduced mass by x due to the flows $Q_{A,B}$ through the servo valve. Thereby, the servo valve is displaced by y through the current i and supplied by the constant pressures $p_{S,T}$.

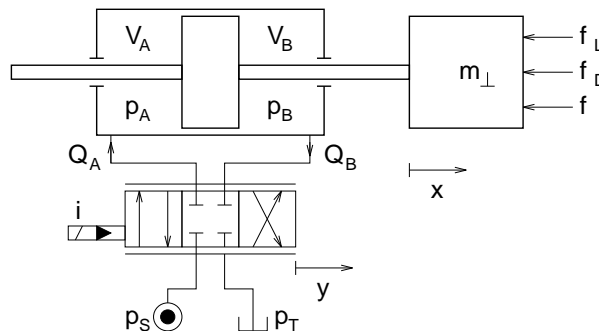


Figure 5: Simplified model sketch

3.2 Linear Model

The transfer function

$$G_H(s) = \frac{X(s)}{Y(s)} = \frac{k_H \omega_H^2}{s^3 + 2d_H \omega_H s^2 + (\omega_H^2 + \omega_A^2)s + \omega_A^2/\tau_H} \quad (14)$$

represents the actuator reaction on the servo valve. The only difference to conventional hydraulic actuation systems is the consideration of the systematic hinge moment [8] by an aerodynamic spring, which yields the additional term, corresponding to the eigenfrequency ω_A [10]. The influence of further aerodynamic loads describes

$$G_F(s) = \frac{X(s)}{F(s)} = \underbrace{k_F (\tau_H s - 1)}_{= G_{PD}(s)} \cdot G_H(s), \quad (15)$$

and

$$G_{SV}(s) = \frac{Y(s)}{I(s)} = \frac{k_{SV}}{\tau_{SV} s + 1} \quad (16)$$

the servo valve dynamics. Figure 6 shows the structure of the transfer function model.

3.3 Parameter Discussion

The parameters of the linear model (14), (15) and (16) concentrate the physical parameters of the nonlinear model, which varies partly within decades. It can be discussed as follows:

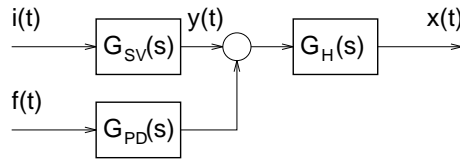


Figure 6: Transfer function description

- d_H : The hydraulic damping depends on the friction of the actuator and the kinematic, the damping constant of the parallel actuators, the flow/pressure characteristic of the servo valve and the leakages between the chambers. It varies mostly because of nonlinear effects of the velocity depending damping and ageing, which is influenced by the over-/underlap of the servo valve. While Taylor linearization leads less effective estimates, nonlinear technics like linearization by harmonic or random describing functions show more realistic results in comparison to the nonlinear time response.
- ω_H : The hydraulic eigenfrequency is a function of the actuator position and the effective/reduced mass of the surface and represents thus the typical nonlinearity. Also it is strongly influenced by the variation of the bulk modulus, which is a linear function of the temperature and a nonlinear function of the chamber pressure.
- k_H : The hydraulic gain is nearly constant in the main range. Only in the narrow area of over-/underlap it is zero/doubled and shows, of cause, saturation characteristic.
- ω_A : According to [8], the aerodynamic eigenfrequency depends on the flight situation: true air speed, flight altitude and air density. But mostly it is proportional to the square of the true air speed, which is nearly zero, for the aircraft rolling on ground.
- τ_H : The hydraulic decay varies on the nonlinear effects of flow/pressure characteristic, inverse proportional like the hydraulic damping.
- k_F : The load gain represents the static effect of actuator displacement on external loads.
- τ_{SV} : The servo valve decay reduces the highly nonlinear and complex dynamic to its first order representation. It varies in a small band, because of internal feedback control.
- k_{SV} : For the variation of the servo valve gain, it is the same as for the servo valve decay.

Table 2 shows the typical value q_i^0 and the extremums of the parameters $q_i^{+/-}$, as well as an heuristic dependency graduation ($-$, o and $+$) on nonlinearity (n.l.) and real parameter variation (var.).

All together the linear model holds eight parameters. It is not necessary to consider all uncertainties, because their effects are only at spacial operation points of interest or they are not really relevant. For an aircraft on ground $\omega_A = 0$ is assumed, because the systematic loads stabilize the surface and this operation point represents the worst case. Hereby the influence of the hydraulic decay τ_H and the load gain k_F in the command transfer function is lost. Also the uncertainty of the

	d_H [-]	ω_H [rad/s]	k_H [m/s]	ω_A [rad/s]	τ_H [s]	k_F [1/m Pa]	τ_{SV} [s]	k_{SV} [m/A]
–	0.01	250	0	0	-0.001	-1.07×10^{-11}	1/250	0.90
0	0.10	350	250	10	-0.015	-8.68×10^{-10}	1/350	1.00
+	0.25	750	500	20	-1.218	-2.20×10^{-9}	1/450	1.10
n.l.	+	+	o	–	+	+	–	–
var.	o	+	–	+	o	o	o	o

Table 2: Parameter uncertainties — values and dependency

servo valve parameters τ_{SV} and k_{SV} are neglected, because they vary in a narrow band, as well as the hydraulic gain k_H inside the saturation. Thus the controller synthesis posses only two relevant uncertain parameters

$$\mathbf{q} = [d_H \ \omega_H]^T. \quad (17)$$

3.4 Discret–time Model

Applying the approximation for time–discretization (5) to the time–continuous model (sec. 3.2) and the extremum assumption for the aerodynamic eigenfrequency (sec. 3.3) yields the time–discrete model

$$\mathbf{A}_d = \begin{bmatrix} 1 & \frac{4T(1+Td_H\omega_H)}{N_1} & \frac{2T^2}{N_1} & \frac{2T^3k_H\omega_H^2\tau_{SV}}{N_1N_2} \\ 0 & \frac{4+4Td_H\omega_H+T^2\omega_H^2}{N_1} & \frac{4T}{N_1} & \frac{4T^2k_H\omega_H^2\tau_{SV}}{N_1N_2} \\ 0 & \frac{-4T\omega_H^2}{N_1} & \frac{4-4Td_H\omega_H-T^2\omega_H^2}{N_1} & \frac{8Tk_H\omega_H^2\tau_{SV}}{N_1N_2} \\ 0 & 0 & 0 & \frac{2\tau_{SV}+T}{N_2} \end{bmatrix}$$

$$\mathbf{b}_d = \left[\frac{T^4k_H\omega_H^2k_{SV}}{N_1N_2} \quad \frac{2T^3k_H\omega_H^2k_{SV}}{N_1N_2} \quad \frac{4T^2k_H\omega_H^2k_{SV}}{N_1N_2} \quad \frac{2Tk_{SV}}{N_2} \right]^T \quad (18)$$

with the abbreviations

$$N_1 = 4 + 4Td_H\omega_H + T^2\omega_H^2 \quad \text{and} \quad N_2 = 2\tau_{SV} + T.$$

Numerical verification for the sample time $T = 1$ ms shows partly remarkable differences between the elements of the exakt and the approximative time–discretization. But this does not really effect the dynamics and the synthesis.

3.5 Controller Synthesis

Avoiding an observer for the servo valve, only an output controller for the states $\mathbf{x} = [x \ \dot{x} \ \ddot{x}]^T$ should be designed

$$\mathbf{k} = [k_x \ k_{\dot{x}} \ k_{\ddot{x}}]^T. \quad (19)$$

Assuming an ideal actuator with a perfect fluid, which yields a pure integral actuator behaviour $G_H(s) \rightarrow k_H/s$, the position feedback gain

$$k_x = \frac{1 - e^{-\omega_B T}}{k_H T} \quad (20)$$

follows directly by the specified bandwidth with the typical value $\omega_B = 2\pi 3\text{ s}^{-1}$ [6]. Besides, this presents a good stiffness against external loads, which is important for the compensation of the systematic hinge moment as well as other additional loads.

Now, the direct pole region assignment (see sec. 2.6) can be applied for the controller synthesis. Therefore the nominal parameter set $\mathbf{q}^{00} = [d_H^0 \ \omega_H^0]^T$ and the two diagonal corners $\mathbf{q}^{--} = [d_H^- \ \omega_H^-]^T$ and $\mathbf{q}^{++} = [d_H^+ \ \omega_H^+]^T$ of the uncertainty domain are chosen as operation points, see table 2. From the time-continuous controller design it is well known that a minimal damping $D^- \approx 0.3$ results good performances. This yields the radius $r = 0.5$ for the boundary $\partial\Gamma$.

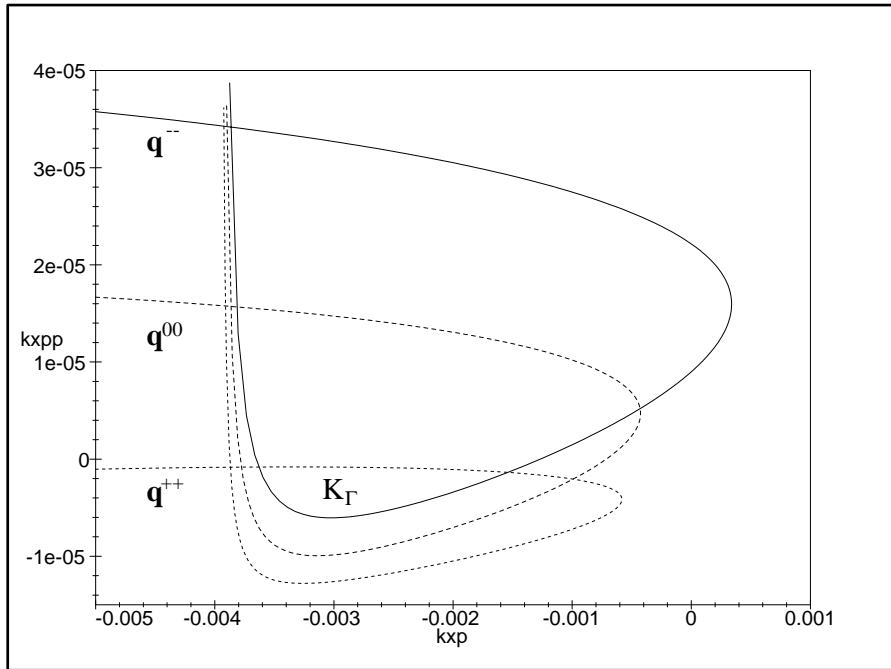


Figure 7: K_Γ region by direct pole region assignment

Figure 7 shows the transformation for the three operation points into the sub-controller space $(k_{\dot{x}}, k_{\ddot{x}})$ — calculated with the computer algebra system *MAPLE V*. Here only the complex boundaries are relevant and the intersection K_Γ is bounded by the two extremum operation points. While the lower bound is formed by \mathbf{q}^{--} , the upper bound by \mathbf{q}^{++} is very close to zero. Thus, for saving needless effort, the acceleration feedback gain will be neglected and the velocity feedback gain is chosen close to the middle between the crossings of the complex boundaries of the two extremum operation points:

$$k_{\dot{x}} = -0.0025 \quad \text{and} \quad k_{\ddot{x}} = 0. \quad (21)$$

This result differs totally from the robust synthesis of the time-continuous controller. In those case the velocity feedback gain can be neglected and the acceleration feedback gain is the decisive one [11, 14].

For the first order differentiation of the position signal, a digital filter of the order $d = 3$ is recommendable. Applying equation (8), yields the sensor transfer

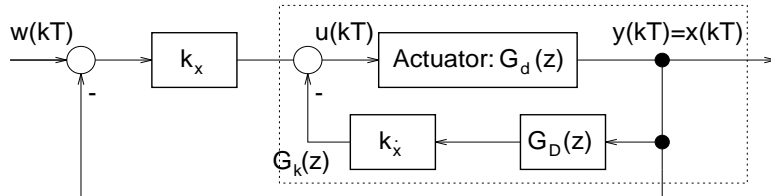


Figure 8: Realized controller structure

function

$$G_D(z) = -\frac{4z^3 - 36z^2 + 36z - 4}{9\pi T z^3}. \quad (22)$$

All together with the velocity feedback gain k_x , it results the structure of fig. 8 for the command transfer function

$$G_W(z) = \frac{k_x G_k(z)}{1 + k_x G_k(z)} = \frac{k_x G_d(z)}{1 + G_d(z) [k_x + G_D(z)]}. \quad (23)$$

3.6 Time-domain Analysis

According to [1], the time-domain test function in the simulations are: demand step of 2.5 % of the maximum displacement x^+ at the time $t = 0.0$ s and load disturbance step of 10 % of the maximum hinge moment at $t = 0.25$ s.

The operation point with a minimum bulk modulus $K_{Oil}^- = 2 \times 10^8$ Pa at the central actuator position $x = 0$ m yields the minimum eigenfrequency ω_H^- of the linear model and it increases with a increasing bulk modulus as well as actuator displacement. The nominal eigenfrequency corresponds to $K_{Oil}^0 = 8 \times 10^8$ Pa as well as $x = 0$ m and the maximal to $K_{Oil}^+ = 17 \times 10^8$ Pa as well as $x \rightarrow x^+$. Additional variations of damping through leakages or the parallel actuator are not examined.

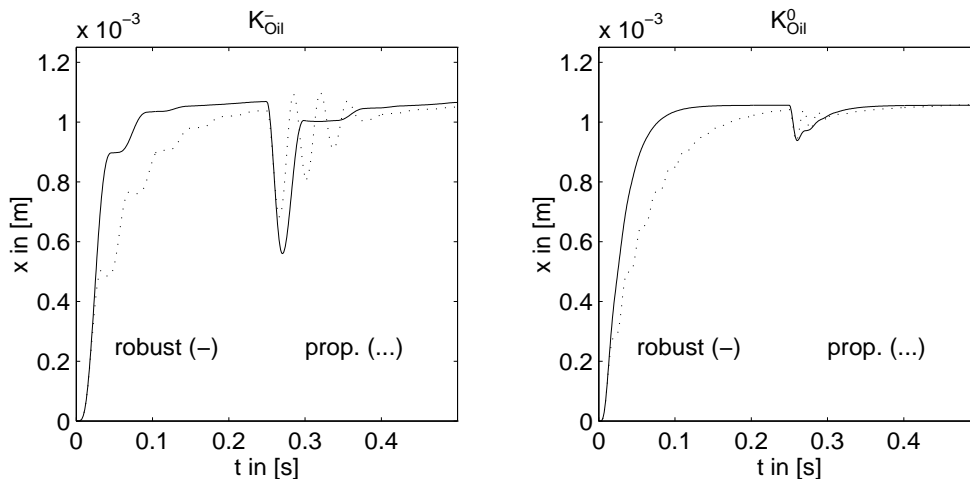


Figure 9: Simulation of proportional and robust controller implementation

Figure 9 compares the actuator with the proportional controller (20) and robust controller extensions (21) and (22) at the two operation points of minimal and nominal bulk modulus. While the actuator with proportional controller in both situations oscillate, with robust controller the responses are much better damped. For

both systems the behaviour improves with rising bulk modulus, this reveals that the operation point with a minimal eigenfrequency is the critical one.

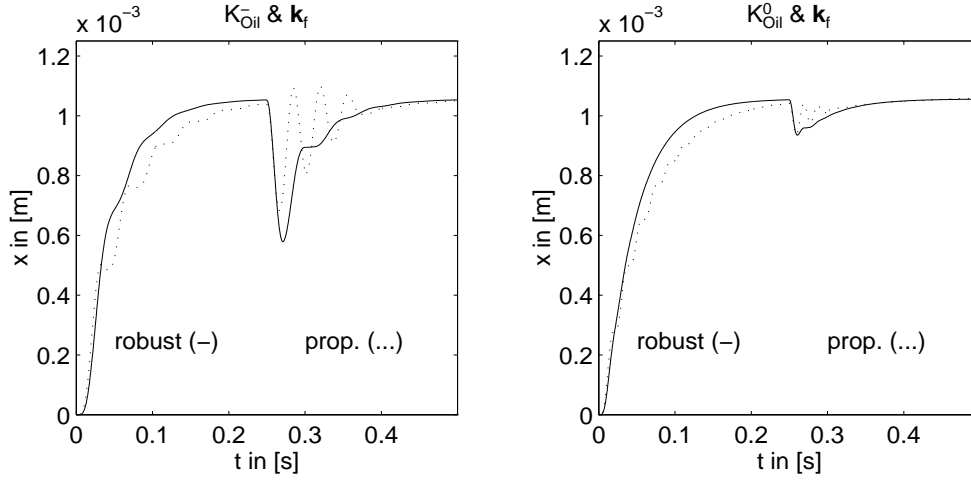


Figure 10: The final controller selection \mathbf{k}_f

The faster response through the robust controller results from the negative velocity feedback gain. This reaction can be compensated in two ways: reducing the velocity or the position feedback gain. Reducing the velocity feedback gain shows a decreasing response, but increases the oscillation. However, reducing the position feedback gain equals the bandwidth and do not increase the oscillations, but it is less stiff against disturbance loads. Thus, a good compromise could be a small reduction of the position feedback gain. Figure 10 shows the responses for the final controller selection

$$\mathbf{k}_f = [2k_x/3 \quad k_x \quad 0]^T \quad (24)$$

in direct comparison to the proportional controller with minimal and nominal bulk modulus.

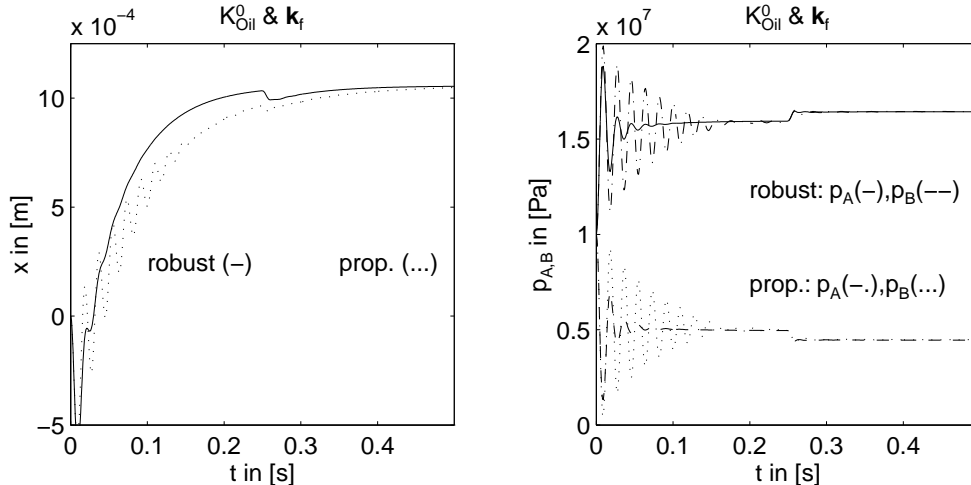


Figure 11: Cruising flight

In the controller synthesis the systematic hinge moment was not respected, but a simulation of a typical cruising flight is here also shown, see fig. 11. Due to the inertial hinge moment of the aileron, which is indicated by the noted pressures

$p_{A,B}$, the actuator undershoots first, reacts slower and oscillates more with both controllers. But the improvement by the robust controller is preserved, also it is indicated by the better damped pressures.

3.7 Frequency-domain Analysis

The differences between the proportional and the robust controlled actuator behaviour can also be seen in the nonlinear frequency responses via correlation analysis [5].

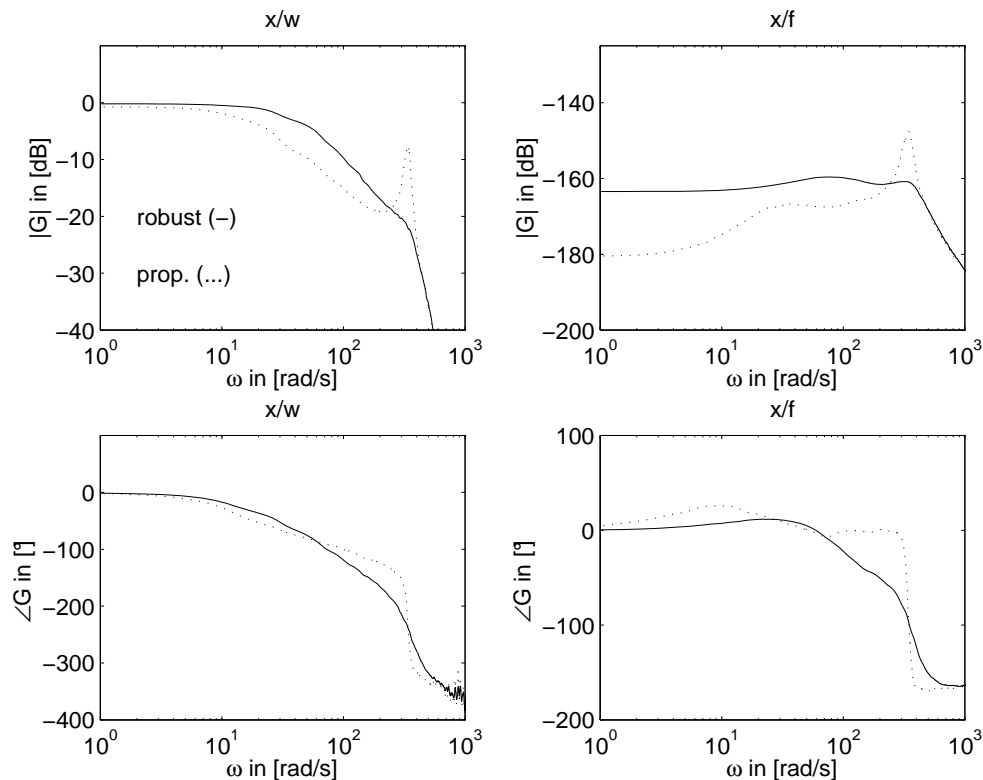


Figure 12: Frequency response

Figure 12 shows the frequency responses of the demand $w(kT)$ and the disturbance input $f(t)$. For the demand input the increasing damping is indicated by cutting off the typical peak in the amplitude and a flatter phase rotation, as well as the faster step response at the upper bandwidth. While the better damped response on the disturbance is caused by the same reasons, the decreasing stiffness, because of the reduced position feedback gain in \mathbf{k}_f , engages the higher amplitude gain for lower frequencies.

Figure 13 shows the frequency responses under cruising flight conditions. Herein the slower step response is indicated by the lower bandwidth.

4 Conclusions

It is presented, how a position controller for the electro hydraulic actuator, applied to a flight control surface, can be synthesized by using the *Parameter Space Design*

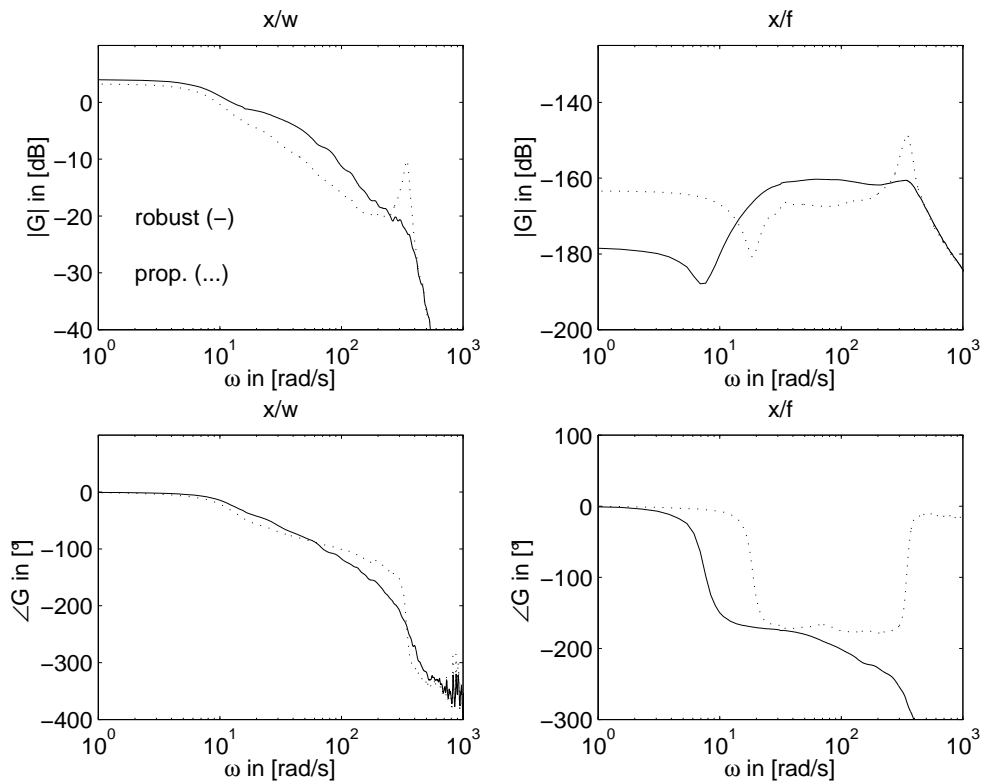


Figure 13: Frequency response under cruising flight conditions

method. Examining the parameters of the linear model on their uncertainties, it results that only the variation of the hydraulic damping and eigenfrequency are relevant for the controller design. The sampled-data design via the direct pole region assignment shows that only one additional feedback gain for the velocity is needed to fulfill the specifications. This is very astonishing, because time-continuous analysis shows the necessity of an acceleration feedback [11, 13, 14]. A digital differential filter generates the velocity signal from the measured regulation variable, the position. The improved positioning behaviour is demonstrated by applying nonlinear simulation, at special operation points and under cruising flight condition for the time as well as the frequency response.

Besides, a nonlinear and robust controller synthesis has been developed and proven by simulation. This allows to compensate e.g. the nonlinear kinematic, if a linear controller does not suffice [15]. Actually, the theoretical results are under verification on a special designed test rig.

In the next step, the elastic dynamics of the control surface should be respected too. Therefore, a multi-body model, developed via finite element discretization, is used to approximate the nonlinear torsion dynamics. Applying order reduction, allows to use the same controller design method. An additional sensor for the angle of torsional surface deflection could help to increase the positioning behaviour of the elastic surface.

Acknowledgment

The author thanks the *Daimler–Benz Aerospace Airbus GmbH* for promoting and supporting the research project *Oszillation elektrohydraulischer Ruderstellensysteme mit digitaler Abtastregelung und dynamischen Störlasten*.

References

- [1] —: *ARP 1281, Actuators: Aircraft Flight Control, Power operated, Hydraulic, General Specification for*. Society of Automotive Engineers Inc., Warrendale, 1993.
- [2] Ackermann, J.: *Sampled–Data Control Systems — Analysis and synthesis, robust system design*. Springer–Verlag, New York, 1988.
- [3] Ackermann, J.; Bartlett, A.; Kaesbauer, D.; Sienel, W.; Steinhauser, R.: *Robust Control — Systems with Uncertain Physical Parameters*. Springer–Verlag, London, 1993.
- [4] Bartley, G.: *Modell 777 Primary Flight Control System*. *Airliner*, Oct.–Dec. 1994.
- [5] Bendat, J.S.; Piersol, A.G.: *Engineering Applications of Correlation and Spectral Analysis*. John Wiley & Sons, New York, 2nd Ed., 1993.
- [6] Bossche, van den D.; et.al.: *Airbus A330/340 Primary Flight Control Actuation System*. SAE Committee A6, Atlanta, 1991.
- [7] Bünte, T.; Siendel, W.: *PARADISE — Eine Matlab–Toolbox für Entwurf und Analyse robuster Regelungen*. *Automatisierungstechnik—at 11/44*, R. Oldenbourg, München, 1996.
- [8] Etkin, B.; Reid, L.D.: *Dynamics of Flight — Stability and Control*. John Wiley & Sons, New York, 3rd Ed., 1996.
- [9] Franklin, G.F.; Powell, J.D.; Workman, M.L.: *Digital Control of Dynamic Systems*. Addison–Wesley, Reading, 2nd Ed., 1990.
- [10] Gee, B.: *The Implications of the Control Surface Actuation System on Flight Control System Design*. In Billings, S.A.; Gray, J.O.; Owens, D.H.: *Nonlinear System Design*; Peter Peregrinus, London, 1984.
- [11] Guillon, M.: *Hydraulic Servo Systems — Analysis and Design*. Butterworths, London, 1968.
- [12] Kliffken, M.G.: *First Progress Report (in German)*. TU Hamburg–Harburg, 23. September 1995.
- [13] Kliffken, M.G.: *Second Progress Report (in German)*. TU Hamburg–Harburg, 1997.
- [14] Kliffken, M.G.; Kruse, U.: *Robust Control of Electrohydraulic Actuators in Primary Flight Control with Special Respect to Sensor Failures (in German)*. To appear in: *Automatisierungstechnik — at*, R. Oldenbourg Verlag, München, 1997.
- [15] Kliffken, M.G.; Kordt, M.: *Structural Nonlinear State–Feedback Design — Application of Lyapunov’s Direct Method (in German)*. To appear in: *Automatisierungstechnik — at*, R. Oldenbourg Verlag, München, 1997.

- [16] Kammeyer, K.D.; Kroschel, K.: *Digitale Signalverarbeitung*. B.G. Teubner, Stuttgart, 2. Aufl., 1992.
- [17] Raymond, E.T.; Chenoweth, C.C.: *Aircraft Flight Control Actuation System Design*. Society of Automotive Engineers Inc., Warrendale, 1993.